Postprint of: Miśkiewicz M., Bruski D., Chróścielewski J., Wilde K., Safety assessment of a concrete viaduct damaged by vehicle impact and an evaluation of the repair, Engineering Failure Analysis, Vol. 106 (2019), 104147, DOI: 10.1016/j.engfailanal.2019.104147

Safety assessment of a concrete viaduct damaged by vehicle impact and an evaluation of the repair

Mikołaj Miśkiewicz[1], *Dawid* Bruski[1*], *Jacek* Chróścielewski[1], *Krzysztof* Wilde[1]

[1] Gdańsk University of Technology, Faculty of Civil and Environmental Engineering, Department of Mechanics of Materials and Structures, 11/12 Gabriela Narutowicza Street, 80-233 Gdańsk, Poland

Abstract. Damage to lower parts of viaducts caused by impact from under-passing high vehicles is relatively frequent. One such incident, in which a viaduct was damaged by the impact from a truck with an improperly assembled hydraulic crane, is considered in this work. The analysis is based on a detailed object damage evaluation, 3D laser scanning, and numerical simulations. The aim of the study is to accurately model the vehicle impact into the viaduct's span. The objective is to diagnose internal damage and to assess the proposed repair concept. No other method will allow discovery of the internal damage, including whether the pre-stressing tendons have been damaged or not. The computational model considers non-linear system dynamics including advanced material definition and the technology of tendon pre-stressing. All complex stages of structural assembly are included in the simulations and the extent of bridge damage is diagnosed. This approach makes it possible to reliably restore the collision event and to assess the safety of internal structural parts. The results from the numerical simulation correspond to the damage measured on the full-scale object. The conducted research indicates that tendons were not damaged as a result of vehicle impact. The structure may be strengthened by means of assembling prestressed concrete girders at both ends. This restoring concept is confirmed analytically. The strengthened structure is intended to show an even greater safety reserve. The proposed strengthening substantially improved structural stiffness, significantly reducing concrete damage and tendon stress in the case of a similar impact in the future. The proposed methodology can also help with research and in practice to assess the safety of other similarly struck and damaged bridges.

Keywords: viaduct, bridge-vehicle impact, pre-tensioned concrete, T-shaped beam, LS-DYNA, numerical simulations

1 Introduction

1.1 Problem description

Viaduct damage due to impact from high vehicles is a frequent occurrence. Two impact types are distinguished with regard to bridge structures. The first is a hard impact, when a vehicle hits the viaduct pier or abutment [1,2]. Hard impacts often bring tragic results, even fatalities. These effects can be minimized by means of safety barriers. Limited zones between the pavement edge and the obstacle make it possible to apply concrete barriers of high stiffness and low working width [3,4]. The second, more frequent impact type is an impact from a vehicle into the viaduct span, usually triggered by driver errors, especially in the case of insufficient clearance. This is an example of a soft impact type [2]. The most frequent damage concerns the lower parts of outer girders and the adjacent structural elements [5–7]. It is worth noting that it is difficult to implement impact-oriented design. Some standards may also present underestimated criteria for determining impact forces [8,9].

Nowadays, access to supercomputing power and present-day computational software enables solving problems with detailed insight into sophisticated engineering problems. This is mainly concerned with static, stability [10–13], and dynamic issues [14–17] of highly developed structural systems due to geometric and material non-linearity. Reliable results within a sufficiently low computational time and in an unlimited solution range are accessible due to, e.g. explicit integration procedure of dynamical motion equations. Advanced numerical simulations are extensively used in the field of road and traffic safety, including the assessment of vehicle impacts into bridge structures. While

*Corresponding author: dawid.bruski@pg.edu.pl

permanent development of computational methods is observed, numerical studies of pre-stressed concrete structures under impact loading are still limited [18]. These works mostly concern vehicle impacts into bridge piers, e.g. [19] and often only the parts immediately surrounding the impact location are analysed.

The paper addresses the computational methodology in dynamic problem solving with the use of LS-DYNA in the case of a real impact on the WD-113 concrete viaduct on expressway S6 of the Koszalin-Sianów beltway (Poland). The aim of the paper is to develop a thorough numerical model of a concrete bridge impacted by a moving crane, on the basis of which an assessment of the bridge safety will be performed. This detailed model can provide data about the history of all mechanical parameters of the dynamic process leading to the bridge damage. The objectives are to diagnose internal damage and to evaluate the proposed repair procedure allowing the ordering of quick construction repair works to return the object into use.

The major load-carrying structural elements are pre-cast prestressed concrete T-beams. In the course of construction, the structure was hit twice by an under-passing vehicle. In order to assess internal structural damage and consequently structural safety, a computational model adjusted to non-linear analysis was formed and all assembly stages were considered. Advanced material definition was introduced to the model enabling recreation of the crack morphology. Making use of the validated numerical model, surface damage in-situ inspection, and 3D real-structure laser scanning, an attempt was made to investigate internal viaduct damage. For this purpose, knowing the damage range resulted from the real impact, a numerical simulation was carried out in which the same object response was obtained. The numerical analysis was aimed at virtual reflecting of the effort evolution and the range of impact-made damage. Based on this validated model, the impact process can be recreated and detailed insight into the destruction mechanisms of the bridge can be obtained. This then makes it possible to check internal damage to the structure. Numerical calculations were supported by 3D laser scanning. An additional advantage of such a validated model is the possibility to assess the proposed repair concept. Together, these tasks form a useful, practical, and inexpensive tool to analyse structural damage resulting from vehicle impact and to evaluate repair proposals. It is also important to consider that the allowable diagnostic methods [20–23] are limited in their in-situ use to possibly identifying microscale defects as well.

There is currently a lack of papers which focus on evaluating internal bridge damage using numerical simulations based on the concrete surface damage. In addition, articles analysing vehicle impact into bridge spans using LS-DYNA are limited. An important element in this analysis is the use in the simulations of a non-linear concrete model, tendons tensioning, and coupling the reinforcement to the concrete. This article is based on a real-life example, presenting the usage of numerical methods as a reliable tool for assessing the safety of impacted structures.

1.2 Literature review

The majority of works considering vehicle impacts incorporate the LS-DYNA dynamic explicit code. This software package offers a lot of possibilities, including a vast material models library. Selected examples concerning prestressed concrete structures analysed in the LS-DYNA are presented below.

1.2.1 Concrete model

The thesis [24] is focused on prestressed concrete beams during impact loading. The authors tested several concrete material models. They concluded that in their case, the *MAT_CONCRETE_DAMAGE_PLASTIC_MODEL (*MAT_273) is the most preferable; however, due to technical issues concerning the chosen pre-stressing method, the *MAT_CSCM (*MAT_159) was chosen. The simulation results were then compared with the laboratory test results.

The *MAT_CSCM (*MAT_159) is presented and described in detail in the reports [25,26] and in the LS-DYNA documentation [27,28]. The work [26] includes an evaluation of the *MAT_CSCM (*MAT_159) model by means of correlation with the test data regarding the impact of the vehicle into a 4.9 m long concrete beam and the tests on a concrete bridge barrier. Notwithstanding the fact that this model was evaluated for roadside safety applications, the authors claim it should be applicable to other dynamic problems.

1.2.2 Tendon tensioning

The paper [29] distinguishes the following options for including the initial tension in the tendons: static implicit solution, transient explicit solution, and dynamic relaxation solution. The authors chose and applied the dynamic relaxation option. Two calculation phases were introduced being tendon tensioning and combining it with the concrete structure. The aforementioned methods are suitable for pre- and post-tensioned concrete.

The work [24] presents a different technique of post-tensioning introduction; the authors distinguish four modelling stages: creating the pre-stressing duct, placing the tendon into the duct, tendon tensioning, and grouting of the pre-stressing duct. A “guiding cable” is used in the location of the pre-stressing duct. The pre-stressing cable is placed along this “guiding cable”, incorporating a special contact type. In order to introduce a force into the tendons, the outer beam elements of the pre-stressing wire are modelled by material deformable due to temperature gradients.

In the study [18], the authors introduce the so-called “Spotweld” method. Here, the pre-stressing bars are modelled by beam elements anchored at both ends by means of external anchors. The tendons are assigned the *MAT_SPOTWELD (*MAT_100) model. The force is applied directly into the tendons using *INITIAL_AXIAL_FORCE_BEAM keyword.

It is worth noting that the way the pre-stressing is introduced in the model differs in both pre-tensioned and post-tensioned concrete cases.

1.2.3 Coupling reinforcement to concrete.

Attention should be paid to the issue of coupling rebars or tendons to concrete structures. One approach is to let the beam elements (rebars) and solid elements (concrete) share common nodes. The main drawback here is creating a shared nodes mesh, especially for a complex rebar configuration [29]. Another method, more commonly used in present times, is the constrained formulation, done in order to shape the reinforcement regardless of the concrete structure discretization. For instance, such options are applied in papers [18,24,26,30].

2 Description of the viaduct and the impacts

The WD-113 viaduct (Fig. 1) along the S-6 expressway at km 2+842.39, located near the city of Koszalin (Poland), consists of two independent structures: WD-113L and WD-113P. Both structures were erected in the form of two-span concrete bridges. The total length of the WD-113P object is 48.9 m and the width is 18.95 m. Their major load-bearing elements are T-shaped 24-m long prestressed concrete beams. Twenty T- beams in the spacing from 0.90 to 0.95 m were used in a single span. The width of the flange is constant, equal 0.89 m. The height of the beams is 1.00 m. A reinforced concrete 24-cm slab was erected over the T-beams. The height of the superstructure is 1.24 m. The cross girders are located over the abutments and over intermediate supports. The height of the cross girder over the abutments ranges up to 1.4 m, and over the piers, is 1.1 m. The cross girders are supported on abutments and piers with the use of pot bearings. A direct foundation of the object was designed on reinforced ground.

Fig. 1 General view of the bridge and the location of the impacts.

The WD-113P structure has been damaged due to two impacts. The first, on 10.11.2017, was an impact from a hydraulic lift crane mounted on a truck. This accident damaged the structure substantially. The incident was caused by excessive velocity combined with an inappropriately secured crane. The impact location is shown in Fig. 1 and as a result of this event, the outermost girder was significantly damaged. The second impact took place on 01.12.2017, the consequences of which were scratches to the girder bottoms. The localization of the second impact is near the point of the first impact. The damaged area is shown in Fig. 2 and Fig. 3. Local inspection showed neither unveiling nor damage to the pre-stressing tendons of the girders.

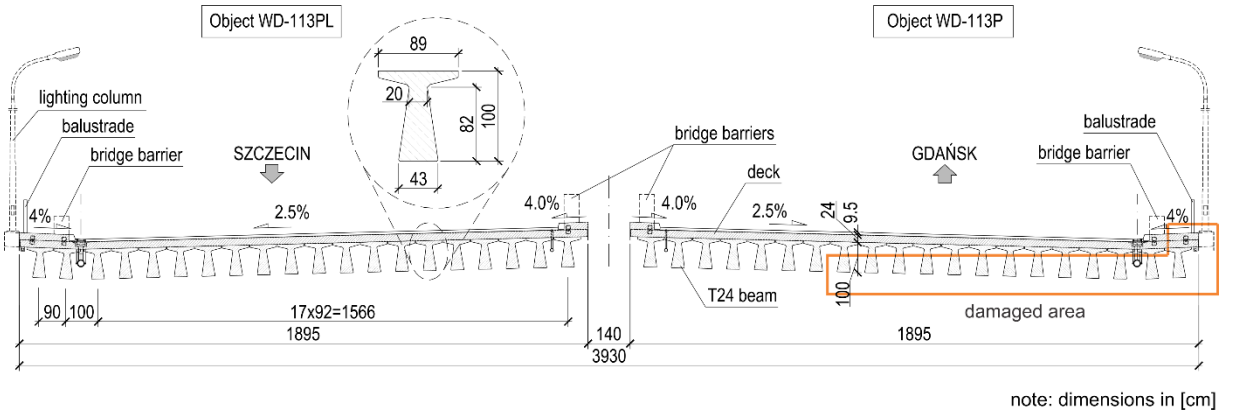

Fig. 2 Cross section of the WD-113 viaduct.

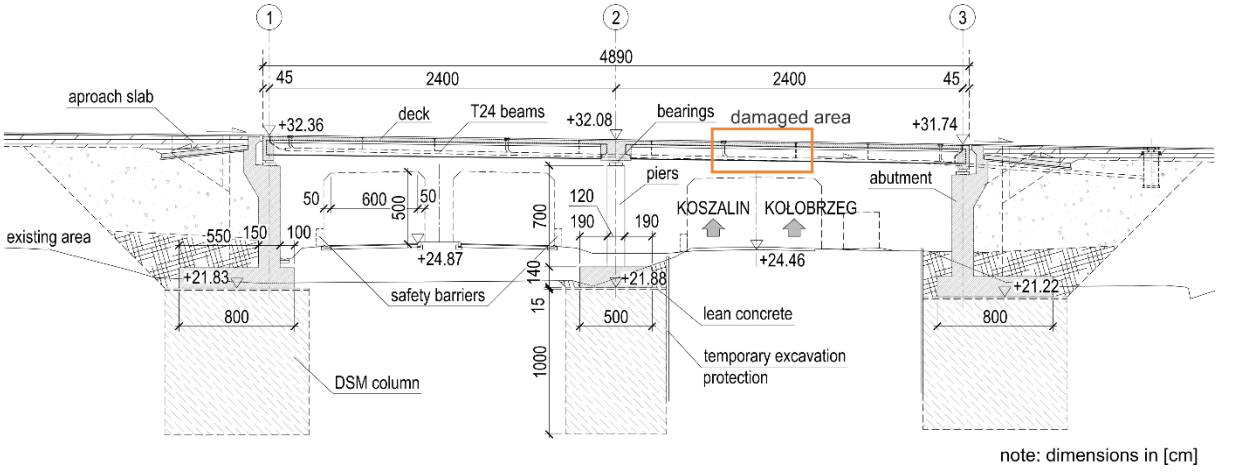

Fig. 3 Side view of the WD-113 viaduct.

3 Measurements of bridge damage

On 15.01.2018 an in-situ inspection was carried out in order to assess the damage caused by the vehicle impacts. The scope of the works included:

- detailed photographic documentation of the object and damage,
- inventory of structural damage including scratch measurements,
- detailed measurements of structural geometry carried out using a laser scanner.

The magnitude of viaduct damage measured during the on-site visit is shown in Fig. 4. The following impact damage effects were observed: loss of concrete in the impact location, significant cracks under the girder flange on both sides, diagonal cracks on both sides of the impact location and a hairline crack on the upper side of the slab, between the two outer T-beams. Cracks were also recorded between the web and the flange in the girder interior (Fig. 4, cross section 3-3, bottom view). During the local inspection, the discrepancies of pre-stressing tendons were not observed. Fig. 5 presents the damage overview. As a result of the second impact, the first 13 beams of the object were scratched. The view of the scratches for the first 5 girders is presented in Fig. 4, section 3-3, while the damage photo is included in Fig. 5e.

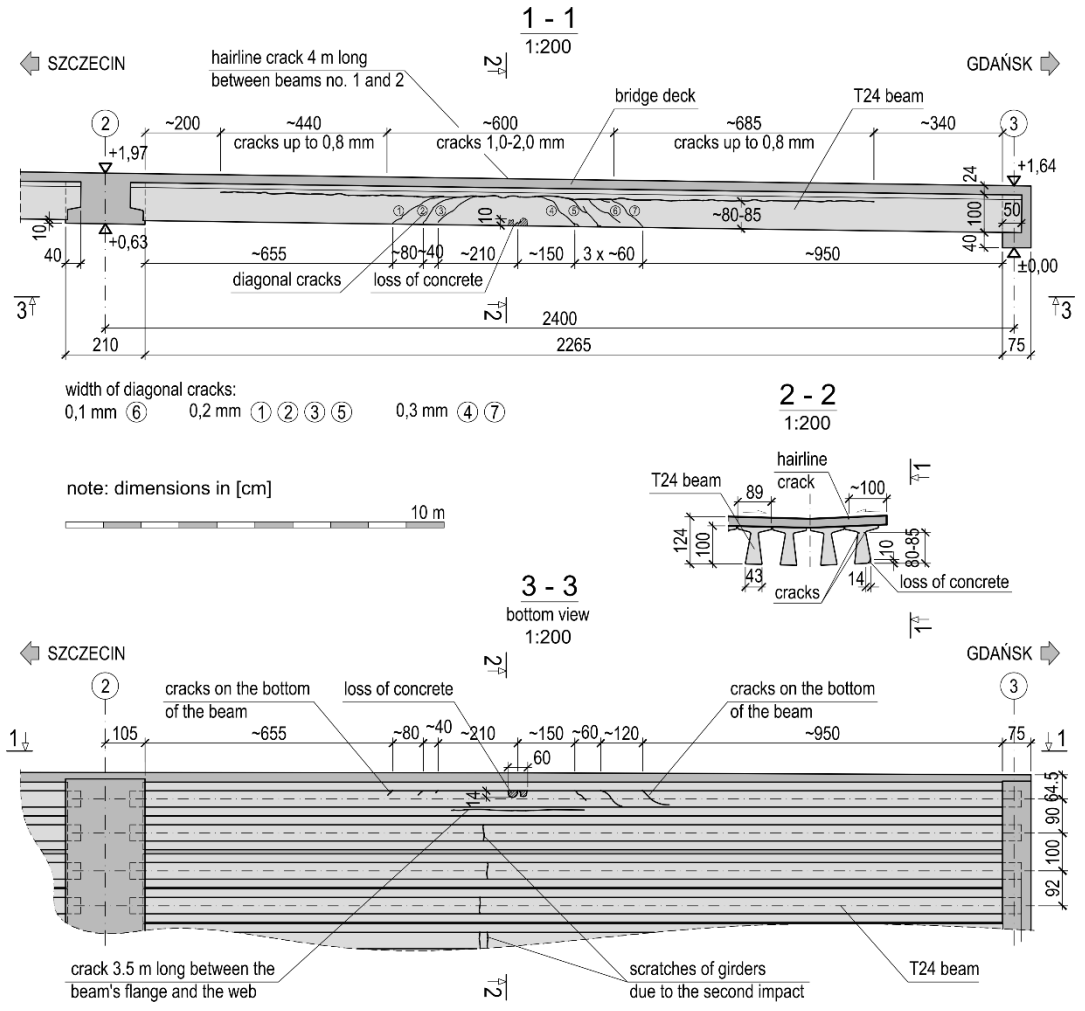

Fig. 4 The damage to the viaduct measured during the on-site visit.

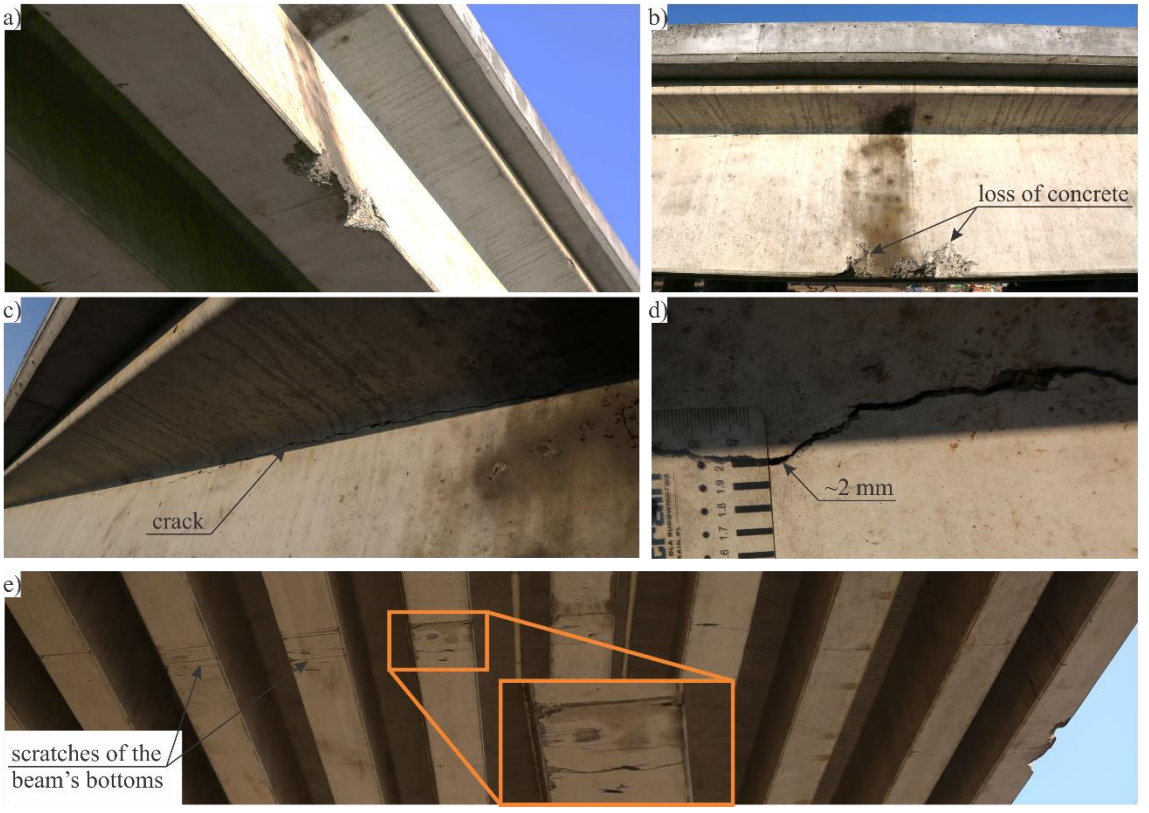

Fig. 5 The damage to the viaduct, a, b) loss of concrete (first impact), c, d) crack under flange (first impact), e) web scratches (second impact).

4 Measurement of bridge geometry

The post-impact geometry of the bridge was surveyed using the Leica P30 3D laser scanner (Fig. 6), similar to the presented method in the articles [31–35]. The cross-section was analysed in detail and the straightness of each girder was checked in order to detect any permanent deformation caused by impact. The analysis did not show any significant differences between the struck WD-113P object and the reference WD-113L structure. Laser scanning showed no changes in the viaduct geometry due to vehicle impact.

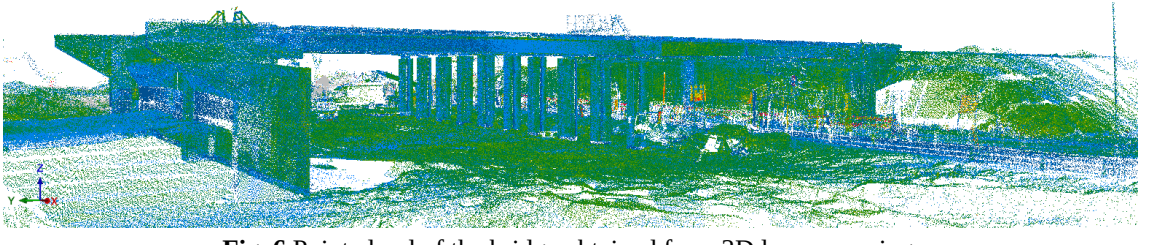

Fig. 6 Point cloud of the bridge obtained from 3D laser scanning.

5 Numerical simulation

5.1 The LS-DYNA application

The quasi-static problem analysis apparently neglects inertia and damping forces. However, these issues are substantial in general dynamic inquiries. LS-DYNA is a renowned, widespread computational tool used to analyse a variety of dynamic actions and featuring highly variable wave propagation induced by explosions, impacts, etc. including the so-called crash tests [36–40]. The LS-DYNA system is adjusted to dynamic analysis, incorporating

integration of motion equations by means of explicit or implicit procedures in both single- and multi-step versions of the letter *a* type (acceleration-oriented).

The calculations within this work were conducted using LS DYNA Finite Element Method code (explicit scheme - central difference method), solver version MPP double precision R10.1.0. The calculations were performed on the supercomputer Tryton, managed by the Academic Computer Centre (CI TASK) in Gdańsk (Poland).

The semi-discrete equation of motion at time *n* reads [27]:

$$Ma^n = P^n - F^n + H^n, \tag{1}$$

where M denotes the diagonal mass matrix, a^n is the nodal acceleration vector, F^n is the vector of nodal point forces equivalent to the element stresses, and H^n is the hourglass resistance. In order to update the nodal velocity vector v and the nodal displacement vector u to time instance t^{n+1}, central difference time integration is conducted:

$$a^n = M^{-1}\left(P^n - F^n + H^n\right), \tag{2}$$

$$v^{n+\frac{1}{2}} = v^{n-\frac{1}{2}} + a^n \Delta t^n, \tag{3}$$

$$u^{n+1} = u^n + v^{n+\frac{1}{2}} \Delta t^{n+\frac{1}{2}}, \tag{4}$$

$$\Delta t^{n+\frac{1}{2}} = \frac{\Delta t^n + \Delta t^{n+1}}{2}. \tag{5}$$

The applied explicit method is conditionally stable. In order to assure solution stability, the integration time step should not exceed a given critical value related to the time of the sound wave passing through a finite element and is described by the following relation:

$$\Delta t = \alpha \Delta t_{crt} \le \min_e \frac{l_e}{c_e}, \tag{6}$$

where α is a Courant number, l_e - characteristic length of a finite element, c_e – velocity of a sound wave in a material.

The important problem addressed in the paper is the selection of a so-called "optimal" size of the numerical model of the bridge. It is necessary to minimize the number of the FE model nodes, minimize the computation time (e.g., rationally select the modelling methods for key nonlinear problems) and maximize the accuracy of the numerical data necessary for detailed damage assessment. The constraints have been set as follows: number of FE model nodes should not exceed 1.5 million nodes, computation time should be shorter than 24 hours on available supercomputer (1.47 PFLOPS), and the size of the FEM element at the damage zone should be in the order of 25 mm to properly capture the damage geometry.

Because of the fact that in the work LS-DYNA is employed as simulation software, all specific terms used below are described in accordance with the names from the LS-DYNA manuals [27,28,41].

5.2 Numerical model of viaduct

In order to assess structural safety, a detailed numerical model was created to serve as a basis for simulation. The bridge geometry was described in the computational model on the basis of design documentation [42]. System discretization marks the number of nodes as equal to 1305079 and the number of finite elements equal to 1056732 (635554 solids, 421178 beams). The overall view of the computational model of the WD-113P viaduct is displayed in Fig. 7.

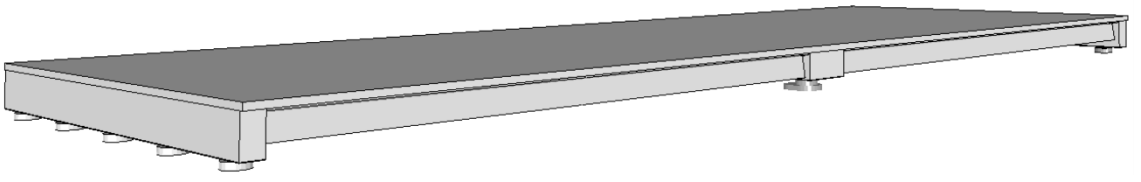

Fig. 7 Overall view of the computational model of the viaduct WD-113P.

5.2.1 Concrete elements

The structure features 20 pre-stressed T-shaped concrete beams assembled with an RC slab. The beams are supported on RC cross girders – two outer, 0.75 m wide and 1.4 m deep, and one intermediate, 2.1 m wide and 1.1 m deep. In the numerical model, the real structure is simplified by means of horizontal, planar geometry modelling, neglecting structural slopes. The outer cross girders are supported on the bridge abutment, while the intermediate cross girder is supported on the columns. The upper part of the columns are modelled only. The supporting of the superstructure on the columns and the abutments is conducted by means of the pot bearings. The connections between the concrete elements are realized by friction forces and by reinforcement that connects these concrete parts. The viaduct modelling procedure made it essential to discretize the system as the efficiency and speed of the central difference method computation is highly affected by finite element dimensions. Fig. 8 compares the numerical model with the real bridge structure.

Fig. 8 Comparative views of the viaduct, a) side view, b) bottom view, c) detail of the structural support.

The concrete structure is discretized by means of a hexahedron shape with the ELFORM = 1 code (constant stress solid element). The outer beam subjected to impact is modelled with very high accuracy. In this case, solid finite elements were applied whose side in the impact zone is approx. 25 mm long, whereas, further away the side is approx. 50 mm long (Fig. 9, upper beam). The outer girder includes 267786 nodes and 237576 solid finite elements. The next, second girder is modelled by means of a sparser FE mesh whose side is approx. 100 mm long (Fig. 9, intermediate beam). The next beams (Fig. 9, bottom) are modelled as solid elements approx. 200 mm long. The sparse mesh in the latter cases results from the higher distance of these elements from the impact spot. A sparse mesh substantially reduces the number of finite elements; hence, computations are faster. The bridge slab is modelled by elements approx. 80 mm long in the impact zone (above the two end girders) and approx. 120 mm long otherwise, in more distant zones.

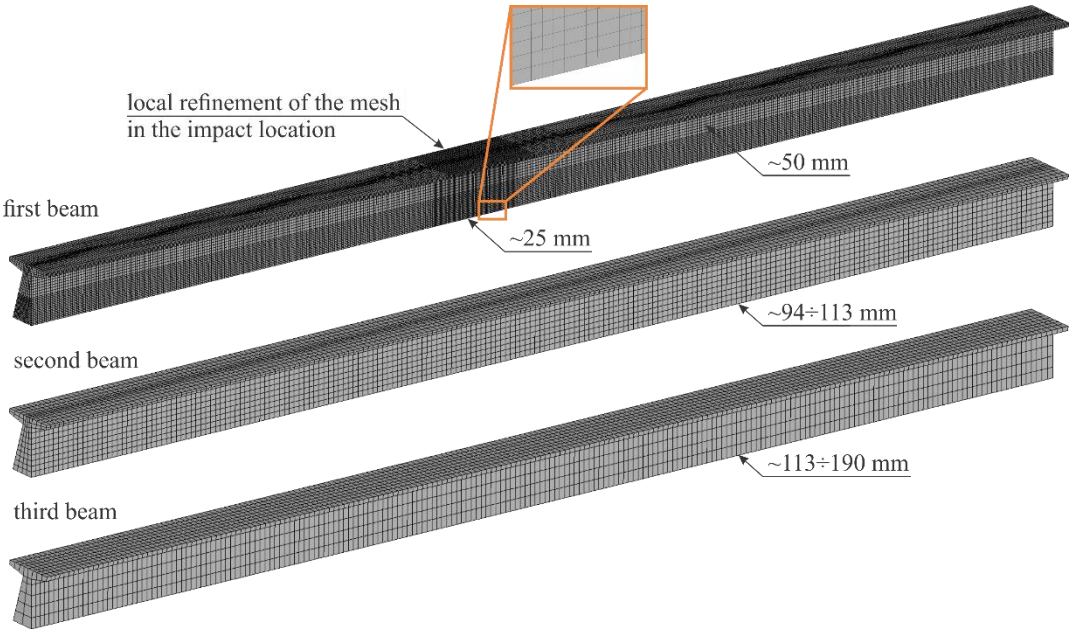

Fig. 9 Details of the model discretization

Due to the concrete structure, the *MAT_CSCM (*MAT_159) concrete model is applied. This material model enables recreating the crack morphology and accurately reflecting concrete damage. It is a highly advanced model whose theoretical background is included in [25–28]. The pre-stressed beams are made of C35/45 concrete, while the cross girder and bridge slab are C30/37 concrete. The key parameters of the two concrete classes listed above are included in Table 1. This model also includes rate effects. The ERODE parameter equal to 1.1 is determined on the basis of the publication [26]. As noted in this work, setting such a value may lead to accumulation of severe damage to be maintained before erosion of the finite elements occurs. An additional reason for setting this value is the formation of a gap of the dimension of the eroded element, the gap width is much larger than the width of the crack.

Table 1 Parameters of *MAT_CSCM (*MAT_159) material model.

Variable	Description	C30/37 (cross girders, slab)	C35/45 (T24 beams)
RO	Mass density	2.300e-09	2.300e-09
NPLOT	Maximum of brittle and ductile damage	1	1
INCRE	Maximum strain increment for sub-incrementation	2.041e-05	2.041e-05
IRATE	Rate effects options	1 (turned on)	1 (turned on)
ERODE	Elements erode when damage exceeds 0.99 and the maximum principal strain exceeds ERODE-1	0.0	1.1 [26]
RECOV	The modulus remains at the brittle damage level	1.0	1.0
ITRETRC	Cap retraction option	0 (not retract)	0 (not retract)
G	Shear modulus	1.146e+04	1.206e+04
K	Bulk modulus	1.255e+04	1.321e+04

The cross girders are simplified in the model, the lower layer is modelled by finite elements of a 20 mm depth and was assigned the *MAT_RIGID (*MAT_020) material model. This operation prevents the cross girders from damage due to self-weight as well as reducing the number of finite elements, possibly necessary to provide reinforcement. This rigid material is very cost efficient [28]. The material density corresponds to the value assumed in the model *MAT_CSCM (*MAT_159) and equals 2300 kg/m^3.

The superstructure is placed on columns and circular-shaped abutment parts via pot bearings. Only the upper parts of the columns and abutments are modelled, solid tetrahedral elements were applied here. The material for these supports was assumed as *MAT_RIGID (*MAT_020), applying constraints (CMO option). The x, y and z

displacements and rotations are constrained. This action assumes the overall supporting conditions of the structure. The upper column parts are shown in the right-hand part of Fig. 8. The pot bearings are described in section 5.2.2.

5.2.2 Steel elements

The model considers steel reinforcement. There are both longitudinal and lateral reinforcement bars as well as tendons in the pre-stressed girders. The reinforcement model is assumed as a slab and pre-stressed girders. The slab reinforcement is modelled in the impact affected zone (ranging to 2.8 m from the plate edge). The reinforcement and pre-stressing tendons considered in the model are presented in Fig. 10.

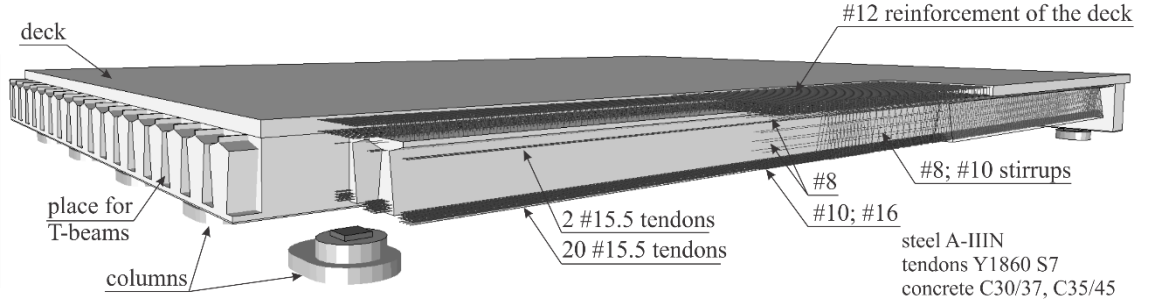

Fig. 10 Details of FEM model, note: only the structural part is displayed due to visibility.

Reinforcement of the girder includes 22 pre-stressing tendons made of Y1860 S7 steel (20 in the lower part, 2 in the upper) of a 141.5 cm^2 cross-sectional area; longitudinal reinforcement made of AIII-N steel (the diameter of the rods is 8 mm, 10 mm, and 16 mm, respectively); lateral reinforcement (stirrups) made of AIII-N steel (with diameter of 8 mm and 10 mm). The stirrup distance is variable along the beam length. The reinforcement layout is presented in Fig. 11. Discretization of structural reinforcement and pre-stressing tendons is made by means of Hughes-Liu beam-type elements (ELFORM=1). The length of a single beam element to model the tendons is 25 mm in the case of the end girder subjected to impact. In the case of other girders, the length is 100 mm. Longitudinal reinforcement is modelled by means of beam elements 100 mm long. The beam elements modelling stirrups have a variable length, equal to approx. 25 mm in the bent rod sections and approx. 50 mm on the linear rod sections. These parts are assumed to be an elastic-plastic model *MAT_PIECEWISE_LINEAR_PLASTICITY (*MAT_024) which considers strain rate (Cowper-Symonds model). It is essential in highly variable and dynamic phenomena. The strain rate is accounted for by scaling the yield stress with the factor calculated by the formula:

$$\beta = 1 + \left(\frac{\dot{\varepsilon}}{C} \right)^{\frac{1}{P}}, \tag{7}$$

where $\dot{\varepsilon}$ stands for the strain rate and C and P are the Cowper-Symonds constants. In the model C =40.4 s^{-1} and P =5 [18,36]. The following reinforcing steel parameters are assumed: mass density 7850 kg/m^3, Young's modulus 210 GPa, Poisson's ratio 0.3, yield stress 500 MPa, and tangent modulus 750 MPa.

The model considers tendon pre-stressing in T-beams, incorporating the method presented in [29], to be further considered in section 5.3.2. The pre-stressing tendons parameters are: mass density 7850 kg/m^3, Young's modulus 195 GPa, Poisson's ratio 0.3, and yield stress 1860 MPa. The detailed reinforcement layout (Fig. 11) is generated for both end girders in the location of the impact. Modelling of other girders is simplified by reducing the number of stirrups and longitudinal bars, but the number of pre-stressing tendons (the main-carrying members) remains unchanged. The overall layout of reinforcement introduced into the model is displayed in Fig. 12.

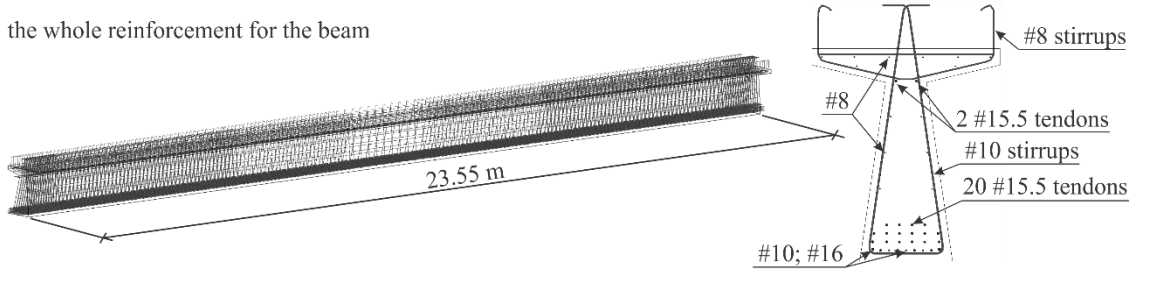

Fig. 11 Detail of the reinforcement of the T24 beam.

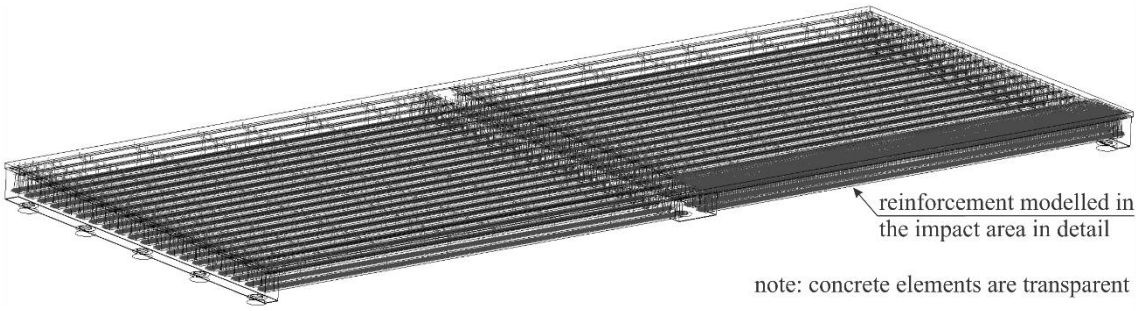

Fig. 12 Reinforcement and tendons in the viaduct computational model

The pot bearing between the cross girders and the column and abutments is modelled by solid hexahedral elements. The bearing material is assumed as *MAT_RIGID (*MAT_020), its density equals 7850 kg/m^3, Young's modulus 210 GPa, and Poisson's ratio is 0.3. The pot bearings can move freely between the superstructure and the supports; the only thing providing supports-bearings-superstructure cooperation is the friction force.

5.2.3 Other model parameters

In the simulation, the stiffness hourglass control (type 2, Flanagan-Belytschko) is used to eliminate zero-energy forms. The hourglass coefficient (QH) equals 0.03.

In the model, the Coulomb friction coefficient is computed by the following formula:

$$\mu = \mu_d + (\mu_s - \mu_d) e^{-c|v|}, \tag{8}$$

where μ_d is dynamic friction coefficient, μ_s is static friction coefficient, c is a decay constant and $v = \Delta e / \Delta t$, where Δe is the incremental movement of slave nodes, and Δt is the time step.

The contact between steel parts (surfaces) is defined by means of *CONTACT_AUTOMATIC_GENERAL keyword. The friction coefficients between steel parts equal $\mu_s = 0.78$; $\mu_d = 0.42$, and $c = 0.001$, respectively [27]. The contact of concrete elements and mutual contact of other elements is defined by the *CONTACT_AUTOMATIC_SINGLE_SURFACE card involving the friction coefficients $\mu_s = \mu_d = 1.8$ [43].

The co-operation of reinforcing steel and pre-stressing tendons with concrete is modelled by the card *CONSTRAINED_LAGRANGE_IN_SOLID.

5.3 Numerical simulation of impact

5.3.1 Vehicle

During the real event, a truck with a built-in hydraulic crane hit the pre-stressed girder of the WD-113P viaduct. No detailed data was available on the vehicle and crane, so the geometry of both was not possible to restore. Derivation of an author's model of the selected vehicle is extremely time-consuming and requires detailed information on vehicle structural elements and material parameters and was, therefore, not possible to create for the presented study. Thus, it was decided to use a simplified vehicle model hereafter (Fig. 14b) which includes a vertical structure reflecting the crane and two slabs at the crane base, fastened by four bolts (Fig. 14c). The lower slab reflects the vehicle part on which the crane is assembled. The total height is 1.9 m and the mass equals 18826.5 kg. Vehicle discretization covers 7199 nodes and 5104 elements (800 shells, 4304 solids). The crane and bolts are modelled by solid elements and the two slabs are modelled by shell elements. The *MAT_PIECEWISE_LINEAR_PLASTICITY (*MAT_024) with properties of steel is used for the crane and the slabs. The bolts are modelled by *MAT_SPOTWELD (*MAT_100). The EFAIL parameter value is set to 0.15, enabling the crane to detach from the vehicle, as happened in the real accident.

5.3.2 Numerical simulation and construction stages

The analysis was divided into stages according to the pre-stressed beam manufacturing process, the beam-slab assembly, and finally, the impact. The termination time was equal to 0.15 s. The computational diagram is presented in Fig. 14.

During the first phase, the tendons are pre-tensioned to a force of 140.5 kN using the function *LOAD_NODE_SET. After this simulation, the DYNAIN.ASCII file is created in LS-PrePost. This file includes *INITIAL_STRESS_BEAM information. The calculations of this phase are only aimed at the initialize stresses in the steel tendons. Next, the second simulation is carried out. The input file includes the created file with initial tendons stresses. During the dynamic relaxation (phase 2), the tendons are coupled to the concrete and, at the same time, the weight of the structure is applied – the dead load increases from 0 to its full value in 0.01 s. After the dynamic relaxation, the transient analysis begins (phase 3). While introducing the changes into the model concerning parts other than the steel tendons (e.g. an additional reinforced beam), there is no need to re-calculate phase 1l; the calculation may be started from phase 2. The results due to each phase are discussed in the next sections.

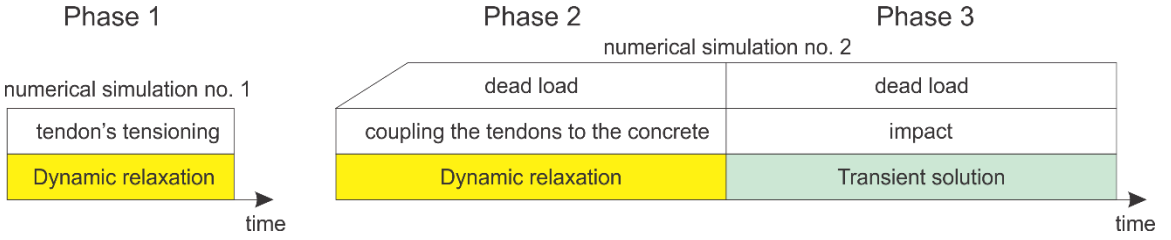

Fig. 13 Numerical simulation phases.

5.3.3 Impact conditions

Due to the lack of relevant data, based on a series of trial tests with reference to the inventoried full-scale structure damage, it was concluded that during perpendicular impact into the viaduct, the speed of an 18.8-ton vehicle should be 50 km/h (Fig. 14a). In addition, the eye-witness statements suggest the vehicle exceeded the speed limit on the road (40 km/h) at the moment of impact, thus, the choice of 50 km/h seems to be reasonable. The simulation considers only the first impact into the viaduct, triggering widespread structural damage. The second impact, producing scratching of the beam-bottom parts, did not affect the structure and was omitted from the analysis.

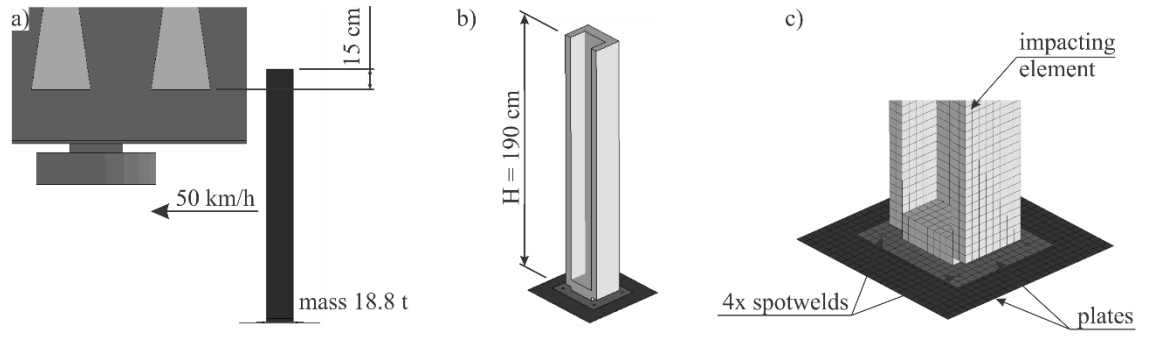

Fig. 14 Vehicle and impact conditions, a) impact conditions, b) simplified model of vehicle and crane, c) details of the vehicle base.

5.4 Simulation results

The simulation was carried out using 24 threads (two 12-core Intel Xeon processors E5 v3 @ 2,3 GHz). The computation time was almost 7 hours. The simulations were conducted according to the stages presented in Fig. 13. Phase 1 covered tendon pre-stressing up to a force of 140.5 kN, corresponding to the value before beam concreting. In this stage, the coupling option of tendons and concrete in a longitudinal direction was inactive, thus, it enabled freely pre-tensioning the tendons. The tendon forces after phase 1 are displayed in the upper part of Fig. 15. A constant force level is achieved along the pre-stressing tendons.

Phase 2 covered the combining of the tendons with concrete, leading to stress re-distribution into the concrete, resulting in tendon force reduction. At this point, the structural self-weight was introduced into the computation. Fig. 15 presents axial forces in the tendons after their assembly with concrete.

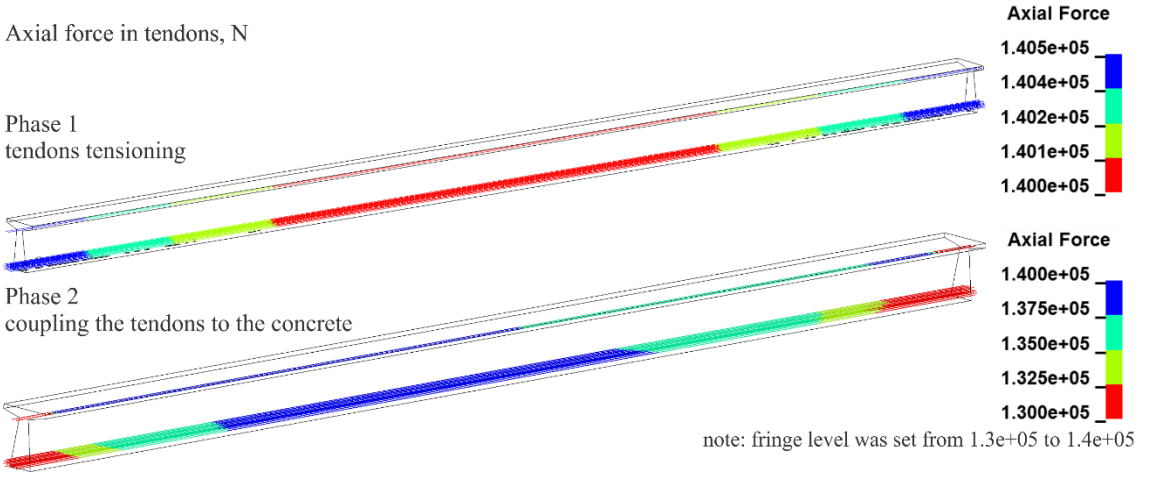

Fig. 15 Axial force in tendons during and after tendon tensioning.

Phase 3 included vehicle entrance and its impact with the girder. The time step was equal to 3.45E-06 s. It was decided that the cracking and damage structural pattern would be represented by the maximum of brittle and ductile damage (NPLOT EQ.1). Fig. 16 and Fig. 17 compare the damage of the real structure with a damage pattern based on numerical simulation. In order to make diagonal cracks more visible in the real structure, Fig. 16a is supplemented by thin black lines coinciding with the cracks. The damage from simulation reflects the damage character from the real structure (Fig. 4), featuring concrete loss on the lower edge, a high-dimension crack under the beam's web, diagonal cracks on both sides of the impact spot, a crack on the upper slab surface between the two outer girders, and a flange-web crack at the internal beam section. The highest forces in the tendons were observed on the internal non-impact side of the web. The maximum axial force in the tendon was equal to 199.6 kN and occurred 0.01 s after the collision. The computations reveal that the forces acting on the tendons during the impact did not exceed the tendon axial load-carrying capacity, i.e. 279 kN. On the basis of these results, it can be concluded that, during the impact, the tendon material performed linearly, thus failure did not occur.

Due to the substantial damage to the concrete, the structure needs strengthening to restore safety levels before it is open to the public again.

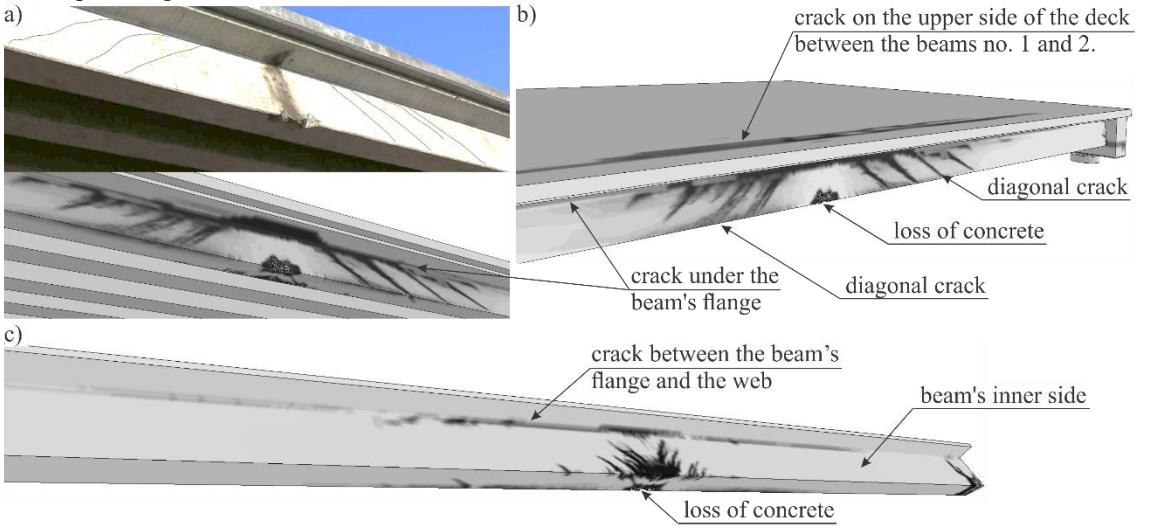

Fig. 16 Damage from numerical simulation, a) overall comparison with real object, b) view from the impact side, c) inner side view - showing only the first beam.

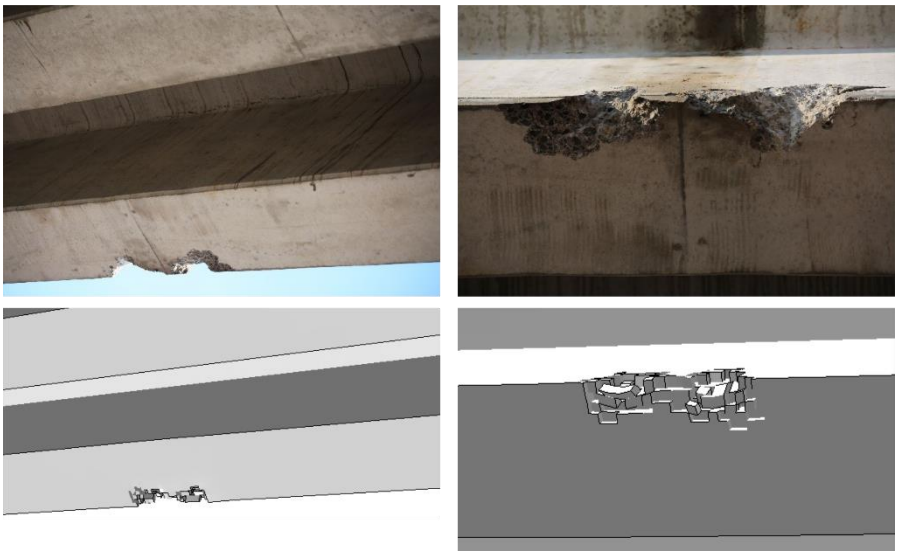

Fig. 17 Detailed damage comparison – the concrete losses (reality on top, simulation below)

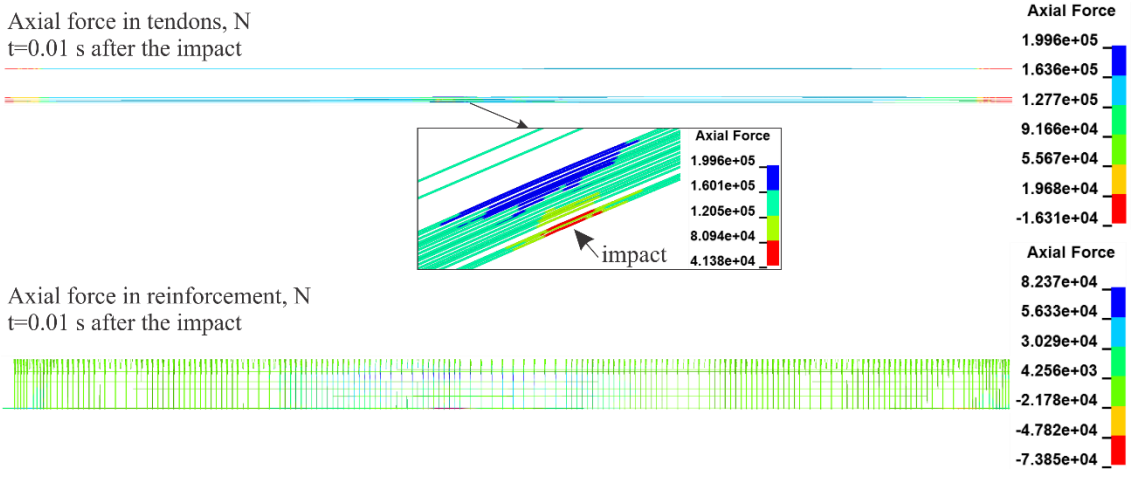

Fig. 18 Axial forces in [N] in the tendons (top) and in the reinforcement and stirrups (bottom).

6 Analysis of the structure after repair

The next computational step was a simulation of a viaduct response to a parametrically identical impact, after the model strengthening proposed by the design team of the general constructor [44]. The strengthening proposition is a monolithic assembly of two end girders by means of introducing an additional adjoining RC beam. The computations were aimed at the assessment of possible damage that may occur in the strengthened structure after a similar vehicle impact in the future.

6.1 Numerical model

The repaired viaduct model includes a number of 1323187 nodes and 1070923 finite elements (646354 solids, 424569 beams). The strengthening concrete is modelled by solid elements ELFORM=1 (constant stress solid element), with a side length of approx. 100 mm. The *MAT_CSCM (*MAT_159) material model is used with properties corresponding to C35/45 concrete (Table 1). The reinforcement is modelled by beam elements with ELFORM=1 formulation (Hughes-Liu with cross section integration). The reinforcement is assigned the *MAT_PIECEWISE_LINEAR_PLASTICITY (*MAT_024) material model. The material properties are assumed as corresponding to AIII-N steel (section 5.2.2). The overall view of the strengthened viaduct is shown in Fig. 19.

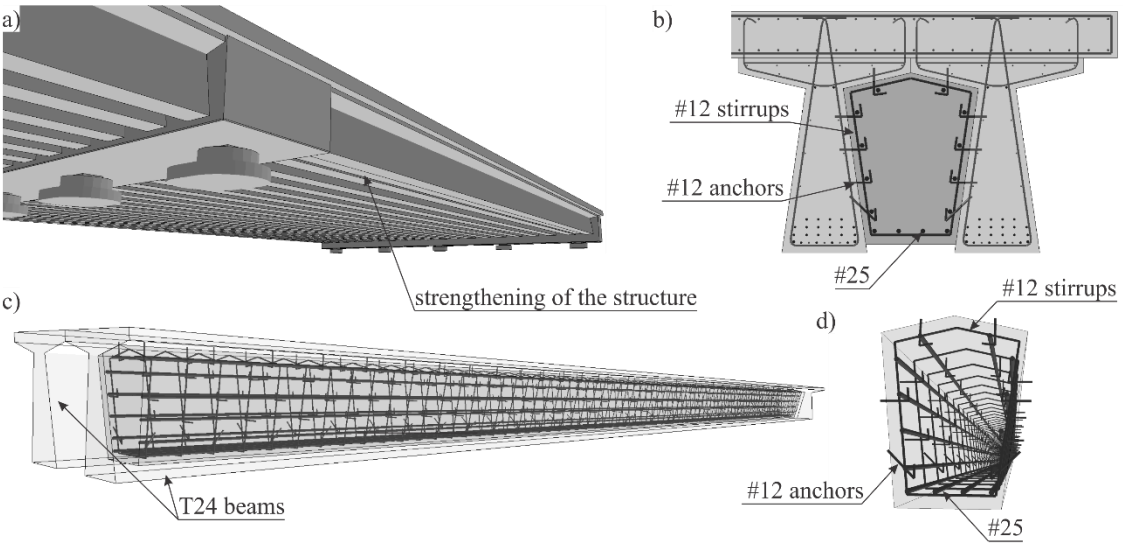

Fig. 19 Bridge structure, a) overall view, b) cross-section, c) view of the reinforcement, d) detail of the reinforcement (only part of the viaduct is presented).

6.2 Numerical simulation

The computations were initiated by phase 2 (Fig. 13), making use of phase 1 from the previous model because the tendon and reinforcement layout did not change. The simulation was conducted using 24 threads (two 12-core Intel Xeon processors E5 v3 @ 2,3 GHz). The time of calculations did not exceed 7 hours.

The vehicle impact causes damage to the outer lower T-beam section, causing cracks around the impact location. A crack emerges under the girder flange; however, much smaller than in the case of the non-strengthened structure. Cracks are also detected on the upper surface of the bridge RC slab, between the two outer beams. No significant cracks resembling the non-strengthened case are observed, including diagonal cracks. Fig. 20 presents an overall damage layout resulting from the impact. The forces in the reinforcement and tendons are presented in Fig. 21. The highest tendon forces occurred in the location closest to the impact, the opposite of what was observed in the non-strengthened structural variant. The maximum axial tendon force appeared 0.01 s after impact, and its value, being 188.3 kN, was lower than the maximum force from the non-strengthened structure.

The simulation shows that the proposed strengthening substantially improved structural stiffness, largely limiting the range of possible damage that may occur in the case of a similar accident in the future.

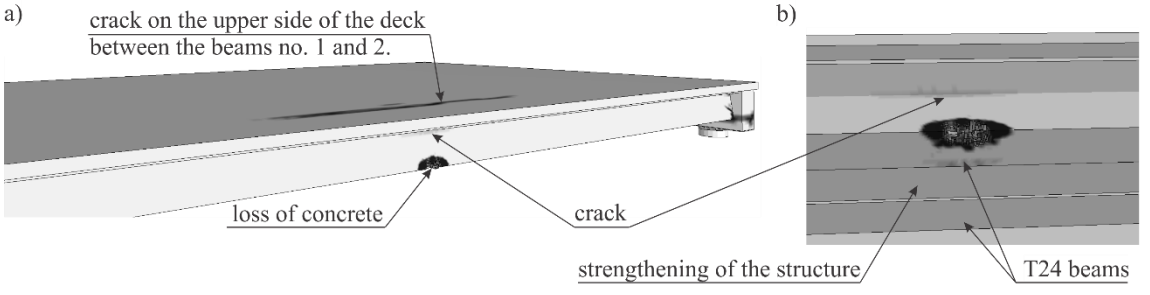

Fig. 20 Result of impact into the strengthened structure, a) overall view, b) bottom view.

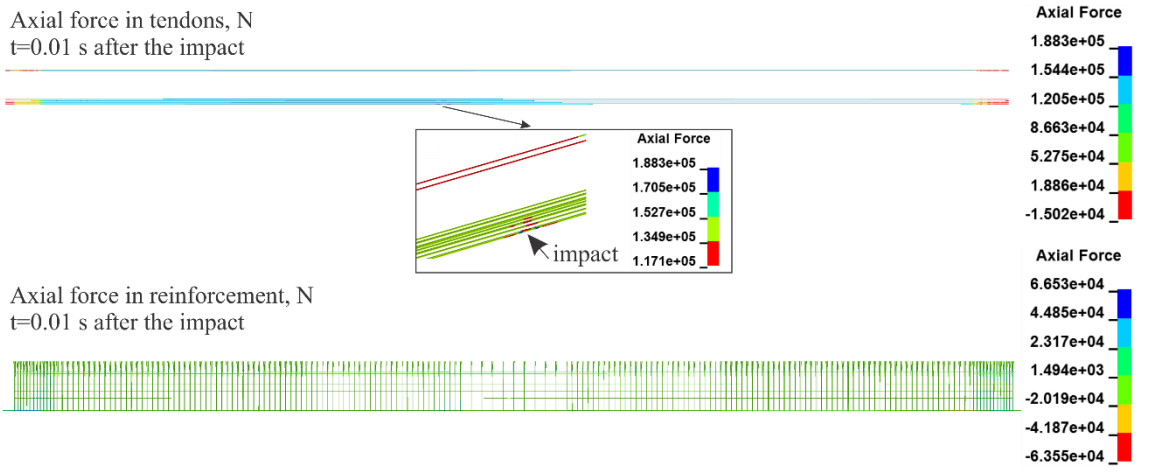

Fig. 21 Axial forces in [N] in the tendons (top) and reinforcement and stirrups (bottom) for strengthened structure.

7 Conclusion

Vehicle impact events on lower girder parts are frequent causes of damage to bridge structures. The potential costs of damaged girder replacement may be enormous and the operation complex due to full structural element assembly and a lack of entirely reliable diagnostic methods to assess internal defects. Nowadays, simulations can help find solutions to these issues. An entirety of highly effective numerical algorithms, structural analysis software, and supercomputer hardware bring an entirely new quality into the processes of design, maintenance, and repair of engineering structures. The explicit procedures and parallel computing performed on high-power machines allow researchers to obtain detailed solutions for complex engineering problems in a relatively short time.

The paper proposes a unique methodology for assessing the internal damage to a concrete bridge resulting from a vehicle impact, which the structure was not designed to tolerate. This technique allows accurate diagnosis of damage to a concrete bridge and, at the same time, allows for a reliable assessment and optimization of the repair concept which not only strengthens the structure but also protects it against similar accidents in the future. This method is based on advanced numerical simulations supported by an extensive in-situ inspection and detailed 3D laser scanning.

The important accomplishment of this study is the creation of a precise model of the concrete pre-stressed bridge that takes into account all stages of bridge construction derived with constraints on FEM model size, computation time, and necessary accuracy of the numerical data for proper damage prediction. The developed model was successfully used to verify the repair concept. The most important conclusions of the work are listed below:

- the proposed assessment methodology allows for a detailed insight into the potential internal damage of the bridge. It turned out that the pre-stressing tendons were not torn and the bridge re-opening for the public requires prior structural strengthening only,
- the numerical model of the bridge-vehicle collision very well describes, qualitatively as well as quantitatively, the real damage done to the WD-113P viaduct,
- the repair should focus on strengthening of the most damaged outer girder which exhibited large cracks and concrete losses triggered by vehicle impact which was not taken into account during the design process,
- the presented concept of strengthening is reasonable due to structural, execution, economical, and operational aspects. Constructing the additional beam after re-profiling and securing the damaged concrete surfaces enables assembling the two end girders. This solution will assure structural safety and protect it from further vehicle impact in the future, the latter having been proved in additional computations. The simplicity of the repair work is another advantage of this option.

Acknowledgements

The computations were carried out at the Academic Computer Centre, Gdańsk University of Technology, Poland.

References

[1] D. Zhou, R. Li, J. Wang, C. Guo, Study on Impact Behavior and Impact Force of Bridge Pier Subjected to Vehicle Collision, Shock Vib. (2017) 1–12. doi:10.1155/2017/7085392.

[2] P. Łaziński, A. Radziecki, M. Salamak, Przestrzenna analiza wytężenia blachownicowych dźwigarów wiaduktów kolejowych uszkodzonych w wyniku uderzenia pojazdów, in: XXV Konf. Nauk. Awarie Bud. 2011, Międzyzdroje, 2011: pp. 1211–1218.

[3] PN-EN 1317-1:2010. Road restraint systems – part 1: Terminology and general criteria for test methods, (2010).

[4] PN-EN 1317-2:2010. Road restraint systems – part 2: Performance classes, impact test acceptance criteria and test methods for safety barriers including vehicle parapets, 2010.

[5] M. Yang, P. Qiao, Analysis of cushion systems for impact protection design of bridges against overheight vehicle collision, Int. J. Impact Eng. 37 (2010) 1220–1228. doi:10.1016/j.ijimpeng.2010.06.007.

[6] P. Qiao, M. Yang, A.S. Mosallam, Impact analysis of I-Lam sandwich system for over-height collision protection of highway bridges, Eng. Struct. 26 (2004) 1003–1012. doi:10.1016/j.engstruct.2004.03.004.

[7] M. Kulpa, T. Siwowski, Failure analysis and repair assessment of a steel box girder bridge, IOP Conf. Ser. Mater. Sci. Eng. 419 (2018) 1–8.

[8] H. Al-Thairy, Y.C. Wang, An assessment of the current Eurocode 1 design methods for building structure steel columns under vehicle impact, J. Constr. Steel Res. 88 (2013) 164–171. doi:10.1016/j.jcsr.2013.05.013.

[9] Y. Sha, H. Hao, Nonlinear finite element analysis of barge collision with a single bridge pier, Elsevier Ltd, 2012. doi:10.1016/j.engstruct.2012.03.026.

[10] P. Szurgott, Modelling and Numerical Analysis of the Reinforced Concrete Viaduct Under the Eurocity EC-114 Train, J. KONES Powertrain Transp. 19 (2012) 515–524.

[11] M. Miśkiewicz, Ł. Pyrzowski, K. Wilde, J. Chróścielewski, Numerical analysis and in situ tests of the Grot Rowecki Bridge in Warsaw, in: Adv. Mech. Theor. Comput. Interdiscip. Issues. Taylor Fr. Gr., London, 2016: pp. 405–408.

[12] Ł. Pyrzowski, M. Miśkiewicz, J. Chróścielewski, The effect of fishing basin construction on the behaviour of a footbridge over the port channel, Polish Marit. Res. Spec. Issue 2017. 24 (2017) 182–187. doi:10.1515/pomr-2017-0037.

[13] J. Chróścielewski, M. Miśkiewicz, Ł. Pyrzowski, B. Sobczyk, Damage Analysis of Tensioning Cable Anchorage Zone of a Bridge Superstructure, Using CDP Abaqus Material Model, Arch. Civ. Eng. 63 (2017) 3–18. doi:10.1515/ace-2017-0025.

[14] M. Gutowski, E. Palta, H. Fang, Crash analysis and evaluation of vehicular impacts on W-beam guardrails placed behind curbs using finite element simulations, Adv. Eng. Softw. 114 (2017) 85–97.

[15] H. Fang, Q. Wang, D.C. Weggel, Crash analysis and evaluation of cable median barriers on sloped medians using an efficient finite element model, Adv. Eng. Softw. 82 (2015) 1–13.

[16] A.O. Atahan, Development of a Heavy Containment Level Bridge Rail for Istanbul, Lat. Am. J. Solids Struct. 15(6) (2018) 1–14.

[17] Z. Ren, M. Vesenjak, Computational and experimental crash analysis of the road safety barrier, Eng. Fail. Anal. 12 (2005) 963–973. doi:10.1016/j.engfailanal.2004.12.033.

[18] D.K. Thai, S.E. Kim, Numerical simulation of pre-stressed concrete slab subjected to moderate velocity impact loading, Eng. Fail. Anal. 79 (2017) 820–835. doi:10.1016/j.engfailanal.2017.05.020.

[19] A. Agrawal, X. Xu, Finite Element Simulation of Truck Impacts on Highway Bridge Piers, 2016.

[20] R. Jasiński, A. Piekarczyk, Ł. Drobiec, Diagnostyka konstrukcji żelbetowych Tom 1. Metodologia, badania polowe, badania laboratoryjne betonu i stali, Wydawnictwo Naukowe PWN, Warszawa, 2010.

[21] M. Rucka, Guided wave propagation in structures, Modelling, experimental studies and application to damage detection, Wydawnictwo Politechniki Gdańskiej, Gdańsk, 2011.

[22] M. Rucka, K. Wilde, Experimental study on ultrasonic monitoring of splitting failure in reinforced concrete, J. Nondestruct. Eval. 32 (2013) 372–383.

[23] M. Miskiewicz, J. Lachowicz, P. Tysiac, P. Jaskula, K. Wilde, The application of non-destructive methods in the diagnostics of the approach pavement at the bridges, IOP Conf. Ser. Mater. Sci. Eng. 356 (2018) 1–8. doi:10.1088/1757-899X/356/1/012023.

[24] A. Johansson, J. Fredberg, Structural Behaviour of Prestressed Concrete Beams During Impact Loading, CHALMERS UNIVERSITY OF TECHNOLOGY (SWEDEN), 2015.

[25] Y.D. Murray, Users Manual for LS-DYNA Concrete Material Model 159, Fed. Highw. Adm. (2007) 77.

[26] Y. Murray, A. Abu-Odeh, R. Bligh, Evaluation of LS-DYNA Concrete Material Model 159, 2007.
[27] J. Hallquist, LS-DYNA, Theory Manual, 2006.
[28] LS-DYNA, keyword user's manual. Vol. II. Material Models, 2015.
[29] L.E. Schwer, Modeling Pre and Post Tensioned Concrete, in: 14th Int. LS-DYNA Users Conf., Dearborn, MI; United States, 2016: pp. 1–22.
[30] A. Maazoun, J. Vantomme, S. Matthys, Damage assessment of hollow core reinforced and prestressed concrete slabs subjected to blast loading, Procedia Eng. 199 (2017) 2476–2481.
[31] M. Przyborski, P. Tysiąc, As-built inventory of the office building with the use of terrestrial laser scanning, E3S Web Conf. 26 (2018). doi:10.1051/e3sconf/20182600011.
[32] J. Szulwic, P. Tysiąc, Searching for road deformations using mobile laser scanning, MATEC Web Conf. 122 (2017). doi:10.1051/matecconf/201712204004.
[33] J. Szulwic, P. Ziolkowski, A. Janowski, Combined Method of Surface Flow Measurement Using Terrestrial Laser Scanning and Synchronous Photogrammetry, Proc. - 2017 Balt. Geod. Congr. (Geomatics), BGC Geomatics 2017. (2017) 110–115. doi:10.1109/BGC.Geomatics.2017.54.
[34] L. Cheng, S. Chen, X. Liu, H. Xu, Y. Wu, M. Li, Y. Chen, Registration of Laser Scanning Point Clouds: A Review, Sensors. 18 (2018) 1–25.
[35] M. Barbarella, A. Di Benedetto, M. Fiani, D. Guida, A. Lugli, Use of DEMs Derived from TLS and HRSI Data for Landslide Feature Recognition, ISPRS Int. J. Geo-Information. 7 (2018) 1–22.
[36] T. Teng, C. Liang, T. Tran, Development and validation of a finite element model for road safety barrier impact tests, Simul. Trans. Soc. Model. Simul. Int. 92 (2016) 565–578.
[37] G. Qian, M. Massenzio, M. Ichchou, Development of a W-Beam Guardrail Crashing Model by considering the Deformations of Components, Proc. 5th Int. Conf. Mechatronics Control Eng. - ICMCE '16. (2016) 42–46.
[38] K. Wilde, K. Jamroz, D. Bruski, M. Budzyński, S. Burzyński, J. Chróścielewski, W. Witkowski, Curb-to-Barrier Face Distance Variation in a TB51 Bridge Barrier Crash Test Simulation, Arch. Civ. Eng. 63 (2017) 187–199.
[39] D. Bruski, S. Burzyński, J. Chróścielewski, K. Jamroz, Ł. Pachocki, W. Witkowski, K. Wilde, Experimental and numerical analysis of the modified TB32 crash tests of the cable barrier system, Eng. Fail. Anal. 104 (2019) 227–246. doi:10.1016/j.engfailanal.2019.05.023.
[40] D. Bruski, S. Burzyński, J. Chróścielewski, Ł. Pachocki, W. Witkowski, On the validation of the LS-DYNA Geo Metro numerical model, MATEC Web Conf. 10001 (2019) 1–6. doi:https://doi.org/10.1051/matecconf/201926210001.
[41] LS-DYNA, keyword user's manual. Vol. I., 2015.
[42] Project: Wiadukt WD-113 w ciągu drogi S-6 w km 2+842,39 opracowany na potrzeby przedsięwzięcia Budowa obwodnicy Koszalina i Sianowa na S-6 wraz z odcinkiem S-11 od węzła „Koszalin" do węzła „Bielice", MP-MOSTY Sp. z o.o., (2015).
[43] PN-B-02003:1982, Obciążenia budowli -- Obciążenia zmienne technologiczne -- Podstawowe obciążenia technologiczne i montażowe, (1982).
[44] Project Wzmocnienie uszkodzonej belki T wiaduktu WD-113, PORR S.A./MOSTY GDAŃSK Sp. z o.o., (2018).